A Robust Double Closed-Loop Control Scheme for PMLSM Drives

MING-YI WANG, YU-JIE NIU, RUI YANG, (Student Member, IEEE), QIANG TAN,
JIA-LIN JIANG, AND LI-YI LI, (Member, IEEE)
Department of Electrical Engineering, Harbin Institute of Technology, Harbin 150001, China

Corresponding author: Ming-Yi Wang (hit_mywang@163.com)

ABSTRACT In this paper, a novel velocity and current double closed-loop control scheme applied to the permanent magnet linear synchronous motor (PMLSM) drives is proposed, and to suppress various uncertainties and disturbances, the advanced observation technique is introduced. First, as the inner loop, the current loop adopts the predictive current control method, which can increase the current control bandwidth and tracking precision. To improve the dynamic response and robustness of the velocity loop, a super-twisting sliding-mode control strategy is presented. Second, to overcome the parameter mismatch issue in the current loop and suppress different force disturbances in the velocity loop, their respective super-twisting sliding-mode observers are structured, and the corresponding estimated values are injected into the double closed loops by the feedforward method. At last, based on the precise PMLSM testing platform, the experimental studies are carried out to prove the effectiveness and correctness of the proposed scheme.

INDEX TERMS Permanent magnet linear synchronous motor (PMLSM), predictive current control, sliding-mode control, super-twisting algorithm, observer.

NOMENCLATURE

v_q, v_d	q- and d-axis voltages.
i_q, i_d	q- and d-axis currents.
R	Phase winding resistance.
L_q, L_d	q- and d-axis inductances.
λ_f	Permanent magnet flux linkage.
λ_q, λ_d	q- and d-axis magnet flux linkages.
v	Linear velocity of the mover.
ζ_q, ζ_d	q- and d-axis disturbance voltages.
T_s	Switching period.
τ	Pole pitch.
p	Pole pairs.
m	Mass of the mover.
x	Displacement relative to the initial position.
F_e	Electromagnetic thrust.
F_{tr}	Thrust ripple.
F_c	Cable disturbance force.
k_f	Thrust coefficient.

I. INTRODUCTION

Compared with most traditional rotary motors, linear motors work with the direct-drive mode, which means the thrust force can be added to the load without the intervention of the mechanical transmission such as gears and ball screws [1]. Therefore, the linear motor system, with the higher acceleration, velocity and accuracy, is being increasingly used in many automatic control systems, such as robots, semiconductor manufacturing equipments, computer numerical-controlled machine tools and X-Y driving devices [2]–[4]. Among all kinds of linear motors, permanent magnet linear synchronous motors (PMLSMs) are particularly suitable for the high-performance automatic control system. Their excellent characteristics, such as high thrust density, high dynamic response, and simple structure, bring higher control performance [5].

Though the direct-drive mode generates many benefits to the linear motor system, it also introduces some inevitable weaknesses. First of all, the adopted control strategies must

meet the rigorous requirement of high dynamic response. Only in this way can the control system have a high bandwidth, and thus improve the control accuracy. In addition, due to the loss of intermediate transmission parts, not only disturbances coming from the motor itself including parameter variation and thrust ripple can directly pass on to the load end, but also external disturbances can be loaded to the motor mover without any damping [6]. Thereby the motion tracking accuracy and stability are drastically reduced. Therefore, it is necessary to focus on the above factors in the controller design of PMLSM drives, and the adopted control strategies should have the features of fast dynamic response and strong robustness to various disturbances.

As the typical structure, the velocity and current double closed-loop control is extensively applied in different linear motor drives. The inner current loop plays an important role in obtaining the precise thrust of PMLSM. At present, three main methods are generally studied in the current loop design. The first one is hysteresis control [7], which is the earliest current control method because of the advantages of fast current response, strong robustness, and simple implementation. But inconstant switching frequency can arouse lots of noise. The second one is proportional-integral (PI) control [8], which has the advantages of the constant switching frequency and high steady state control performance. But if the motor works in different states, variable current tracking commands will decrease the control performance. Additionally, the current loop with the PI controller usually neglects the d-q axis coupling and back electromotive force (EMF) disturbance. Currently, with the development of the digital control, the current loop based on the predictive current control (PCC) [9]–[11] method becomes a strong trend. Compared with the first two methods, PCC has more prominent static and dynamic performance. In theory, the current could track its command after one switching period. Furthermore, because of its model-based principle, PCC can solve the d-q axis coupling and EMF disturbance issues [9]. However, PCC is absolutely dependent on the motor model, and the parameter variations will give rise to the unsatisfactory response, hence many researches focus on the parameter disturbance compensation. In [12], a discrete fuzzy-tuning current vector control method, which only uses the phase current, is presented to solve the parameter sensitivity issue. On the basis of the current error correction technique [13], the current tracking precision and response speed are improved obviously. In [14], the least square method is used to identify the motor parameters. In [15]–[20], the disturbance observer technologies are utilized to suppress the parameter variation. In [15], the time-delay disturbance observer is structured to estimate the parameter variation voltage, but this method is limited because it assumes that disturbance voltages during several adjacent switching periods are approximately constant. In [16], the adaptive internal model theory is studied to design the disturbance observer. Among all kinds of disturbance observers, on account of strong robustness and

fast response, the sliding-mode observer (SMO) is commonly used to overcome the system uncertainty [17]–[20], especially the SMO based on the super-twisting algorithm is proposed to compensate the parameter disturbances for different systems.

As for the motion control system based on the linear motor, the most important issue is how to suppress all kinds of disturbances or system uncertainties, including thrust ripple, cable disturbance, model error, and uncertain load. To improve the motion control precision, the control strategy used in the velocity/position loop must possess the strong disturbance suppression ability. Therefore, a lot of advanced methods have been proposed to satisfy the high requirement of the velocity/position loop. Adaptive fuzzy control [21], adaptive robust control [22], cascaded iterative learning control [23], neural-networks control [24], and sliding-mode control (SMC) [25]–[27] have been developed to improve the control performance in the linear motor drives. Among those methods, SMC, as one of the most robust control methods, is attracting a widespread attention. What is more, it also has the properties of fast response and easy realization. Nevertheless, the main weakness of SMC is the chattering problem. One of the most effective manners for avoiding the chattering is to design the high-order SMC. Since the high-order SMC based on the super-twisting algorithm (STA) has an integrator, the discontinuous signal is smoothed out. Therefore, the super-twisting sliding-mode control (STSMC) can availably attenuate the chattering phenomenon. Reference [28] presents more details about the STSMC, and this strategy has been gradually applied in different control systems [29]–[31].

To realize the high motion control performance of PMLSM drives, this paper proposes a STSMC+PCC double closed-loop control scheme. In the meantime, the high-order sliding-mode observer (HOSMO) based on STA is designed, and the respective disturbance observers of the current and velocity loop are utilized to suppress uncertainties and disturbances. This paper is organized as follows. Section II establishes the discrete-time model of PMLSM considering the parameter variations. Section III presents the STSMC+PCC double closed-loop control method. In Section IV, the principle of the super-twisting sliding-mode observer (STSMO) is discussed, and the different STSMOs are designed to estimate the parameter variations of PCC and the force disturbances of STSMC, respectively. In Section V, the proposed scheme is carried out in a precise PMLSM testing platform. Lastly, Section VI gives the conclusion.

II. PMLSM MODEL
In the synchronous rotating reference frame, mathematically, the dynamic model of a typical PMLSM can be expressed as

$$
\begin{cases}
v_q = R_o i_q + \dfrac{d\lambda_{qo}}{dt} + \dfrac{\pi v \lambda_{do}}{\tau} + \zeta_q \\[3mm]
v_d = R_o i_d + \dfrac{d\lambda_{do}}{dt} - \dfrac{\pi v \lambda_{qo}}{\tau} + \zeta_d
\end{cases}
\tag{1}
$$

where the subscript "o" denotes the nominal value, λ_{qo} and λ_{do} can be given as

$$\begin{cases} \lambda_{qo} = L_{qo}i_q \\ \lambda_{do} = L_{do}i_d + \lambda_{fo} \end{cases} \quad (2)$$

With the motor operation or the change of external condition, the parameters set in the controller may be different from the actual ones. The disturbance voltages of parameter variation can be expressed in the following form.

$$\begin{cases} \zeta_q = \Delta R i_q + \dfrac{\Delta L_q di_q}{dt} + \dfrac{\pi v \Delta L_d i_d}{\tau} + \dfrac{\pi v \Delta \lambda_f}{\tau} \\ \zeta_d = \Delta R i_d + \dfrac{\Delta L_d di_d}{dt} - \dfrac{\pi v \Delta L_q i_q}{\tau} \end{cases} \quad (3)$$

where ΔR, ΔL_q (ΔL_d) and $\Delta \lambda_f$ are the respective variations.

Due to the end and slot effects, generally, the thrust output of PMLSM is not just the electromagnetic thrust. In addition, there is a large thrust ripple. As a parasitic force, the thrust ripple F_{tr} is periodic with the linear position of PMLSM under the ideal conditions. Based on the above analysis, the thrust force is written as

$$F = F_e + F_{tr}. \quad (4)$$

For the surface-mounted PMLSM, it is assumed that $L_{qo} = L_{do} = L_{so}$. The electromagnetic thrust F_e is given by

$$F_e = k_f i_q \quad (5)$$

where $k_f = 3\pi p \lambda_f / 2\tau$.

Since the studied PMLSM is supported by the aerostatic guide, the frictional force can be ignored. In the meantime, the linear motor drives the mover to make the acceleration or deceleration motion, so the external load force is zero. Thereby dynamic equation of PMLSM is written as

$$m\frac{dv}{dt} = F_e + F_{tr} - F_c. \quad (6)$$

If considering those force disturbances, including thrust ripple and cable force, a total force disturbance F_d is defined as

$$F_d = F_{tr} - F_c. \quad (7)$$

The final dynamic equation is described as

$$\dot{v} = \frac{k_f}{m}i_q + \frac{1}{m}F_d. \quad (8)$$

Because of the installation error and other uncertainties, the actual thrust ripple F_{tr} is not completely periodic. In addition, the cable force F_c is nonlinear. So the mathematical model of force disturbance is difficult to establish. Though the force disturbance suppression is a challenging work, it is necessary to consider the force disturbance compensation in the velocity loop design.

III. DOUBLE CLOSED-LOOP CONTROL DESIGN

This paper studies a robust double closed-loop control scheme, as shown in Fig. 1. To improve the motion tracking precision, the current loop adopts PCC, and the velocity loop is based on STSMC. In the meantime, STSMOs are designed to overcome the uncertainties or disturbances in the double closed-loop. On the basis of the space vector PWM technology, the calculated voltage vector is loaded to the PMLSM by using a three-phase voltage source inverter (VSI).
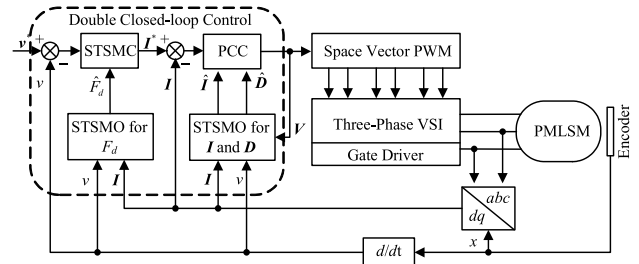

FIGURE 1. Block diagram of the proposed robust double closed-loop control scheme.

A. PCC IN CURRENT LOOP

For the digital implementation of the PCC method, the motor model should be expressed in a discrete-time domain. According to the voltage equation in the continuous domain, its discrete-time form is obtained by means of the first-order Taylor series expansion.

$$\begin{cases} v_q(k) = R_o i_q(k) + \dfrac{L_{qo}}{T_s}\left[i_q(k+1) - i_q(k)\right] \\ \qquad + \dfrac{\pi v L_{do}}{\tau}i_d(k) + \dfrac{\pi v \lambda_{fo}}{\tau} + \zeta_q(k) \\ v_d(k) = R_o i_d(k) + \dfrac{L_{do}}{T_s}\left[i_d(k+1) - i_d(k)\right] \\ \qquad - \dfrac{\pi v L_{qo}}{\tau}i_q(k) + \zeta_d(k). \end{cases} \quad (9)$$

According to (9), the voltage equation is rewritten in matrix form

$$\boldsymbol{V}(k) = \boldsymbol{G} \cdot \boldsymbol{I}(k) + \boldsymbol{H} \cdot \boldsymbol{I}(k+1) + \boldsymbol{\lambda} + \boldsymbol{D}(k) \quad (10)$$

where

$$\boldsymbol{V}(k) = \begin{bmatrix} v_q(k) & v_d(k) \end{bmatrix}^T, \quad \boldsymbol{I}(k) = \begin{bmatrix} i_q(k) & i_d(k) \end{bmatrix}^T,$$

$$\boldsymbol{\lambda} = \begin{bmatrix} \pi v \lambda_{fo}/\tau & 0 \end{bmatrix}^T, \quad \boldsymbol{D}(k) = \begin{bmatrix} \zeta_q(k) & \zeta_d(k) \end{bmatrix}^T,$$

$$\boldsymbol{G} = \begin{bmatrix} R_o - L_{qo}/T_s & \pi v L_{do}/\tau \\ -\pi v L_{qo}/\tau & R_o - L_{do}/T_s \end{bmatrix},$$

$$\boldsymbol{H} = \begin{bmatrix} L_{qo}/T_s & 0 \\ 0 & L_{do}/T_s \end{bmatrix}.$$

Moving the current vector $\boldsymbol{I}(k+1)$ to the left side of the formula, it is expressed as

$$\boldsymbol{I}(k+1) = \boldsymbol{G}_0 \cdot \boldsymbol{I}(k) + \boldsymbol{H}_0 \cdot [\boldsymbol{V}(k) - \boldsymbol{\lambda} - \boldsymbol{D}(k)] \quad (11)$$

Where

$$G_0 = \begin{bmatrix} 1 - R_o T_s / L_{qo} & -\pi v T_s / \tau \\ \pi v T_s / \tau & 1 - R_o T_s / L_{qo} \end{bmatrix}$$

$$H_0 = \begin{bmatrix} T_s / L_{qo} & 0 \\ 0 & T_s / L_{qo} \end{bmatrix}.$$

For the PCC theory, the voltage command $V^*(k)$ is calculated on the basis of (10).

$$V^*(k) = G \cdot I(k) + H \cdot I^*(k+1) + \lambda + D(k) \quad (12)$$

If we can obtain $V^*(k)$ with the known $I(k)$, $D(k)$, and the current command $I^*(k+1)$, and $V^*(k)$ is loaded to the motor at the beginning of the kth period, the actual current will accurately track $I^*(k+1)$ at the end of the kth period. Nevertheless, $V^*(k)$ has to be added to the motor with one period delay in the digital control, which will lead to undesired overshoot or oscillation, so we should avoid this problem. Therefore, we can calculate $V^*(k+1)$ during the kth period.

$$V^*(k+1) = G \cdot I(k+1) + H \cdot I^*(k+2) + \lambda + D(k+1). \quad (13)$$

On this occasion, we have to face the new problems, which are the unknown actual current $I(k+1)$ and parameter disturbance $D(k+1)$. Thus they should be substituted by their estimations, and $V^*(k+1)$ can be rewritten as

$$V^*(k+1) = G \cdot \hat{I}(k+1) + H \cdot I^*(k+2) + \lambda + \hat{D}(k+1). \quad (14)$$

On the basis of the space vector pulse width modulation (SVPWM) technology, $V^*(k+1)$ is loaded to PMLSM at the beginning of the $(k+1)$th period, and the current command $I^*(k+2)$ will be tracked at the end of the $(k+2)$th period. It means that the current command will be tracked after two sampling periods [9], [32]. The timing sequence of the improved PCC is shown in Fig. 2.
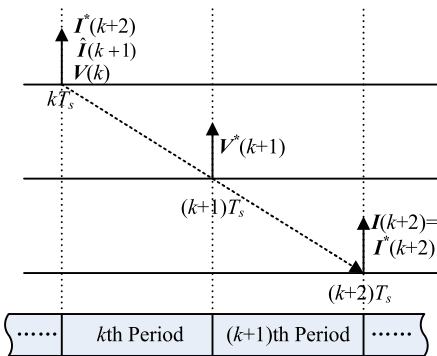

FIGURE 2. Timing sequence of the improved PCC.

B. STSMC IN VELOCITY LOOP

Levant [33] proposed the super-twisting algorithm, then he presented a classical robust exact differentiation [28] by means of this method. Apart from the strong robustness and

fast convergence of SMC, STA also can hide the chattering effect into the high order derivative. Hence we intend to design the STSMC as the controller of the velocity loop.

In [34] and [35], the STA described by the differential inclusion was proposed. Firstly, define the dynamical system in the following form.

$$\begin{cases} \dot{x} = -\alpha_1 |x|^{1/2} sgn(x) + X + \rho_1(t) \\ \dot{X} = -\alpha_2 sgn(x) \end{cases} \quad (15)$$

where x denotes the state variable, α_1, α_2 are gains, and $\rho_1(t)$ is a bounded disturbance, which satisfies

$$|\rho_1(t)| \leq \delta_1 |x|^{1/2} \quad (16)$$

where the constant $\delta_1 \geq 0$. The dynamical system is stable and all trajectories will converge to the origin in finite time if the gains α_1, α_2 meet the following requirements [34].

$$\begin{cases} \alpha_1 > 2\delta_1 \\ \alpha_2 > \dfrac{5\delta_1\alpha_1^2 + 4\alpha_1\delta_1^2}{2\alpha_1 - 4\delta_1} \end{cases} \quad (17)$$

Now, for the velocity controller design, the input command is v^*, and the output command is i_q^*, which is also the input command of the current loop. According to (8), we can define the SM variable and deduce its derivative as

$$\begin{cases} S = v - v^* \\ \dot{S} = \dfrac{k_f}{m} i_q^* + \dfrac{1}{m} F_d - \dot{v}^* \end{cases} \quad (18)$$

If the controller output is designed as

$$i_q^* = \frac{m}{k_f} \left(-\alpha_1 |S|^{1/2} sgn(S) - \int_0^t \alpha_2 sgn(S) d\tau + \dot{v}^* - \frac{1}{m}\hat{F}_d \right) \quad (19)$$

where $\hat{F}_d$ is the estimation of F_d, and substituting (19) into (18), we can obtain the STSMC in the following form.

$$\begin{cases} \dot{S} = -\alpha_1 |S|^{1/2} sgn(S) + S_1 + \dfrac{1}{m}\left(F_d - \hat{F}_d\right) \\ \dot{S}_1 = -\alpha_2 sgn(S). \end{cases} \quad (20)$$

Compared with (15) and (16), it can be seen that if setting $\rho_1(t) = \left(F_d - \hat{F}_d\right)/m \leq \delta_1 |S|^{1/2}$, and the gains α_1, α_2 are chosen in accordance with (17), the designed velocity controller is stable, furthermore, the actual velocity will track its command in finite time.

IV. SUPER-TWISTING SLIDING-MODE OBSERVER

In the design of double closed-loop controllers, there are some unknown variables or disturbances, such as current vector $I(k+1)$, parameter disturbance $D(k+1)$, and force disturbance F_d. Thereby, this part will present an effective observation method on the basis of STA, which can be utilized to estimate unknown variables or disturbances in the proposed controller.

A. THIRD-ORDER STSMO

To express the fundamental of the designed third-order STSMO, the state equations of the observed system are defined as

$$\begin{cases} \dot{x}_1 = x_2 + u \\ \dot{x}_2 = \rho_2(t) \end{cases} \quad (21)$$

where x_1 and x_2 are the state variables, u is the control input. As the derivative of x_2, $\rho_2(t)$ is bounded, which is expressed as

$$|\rho_2(t)| \leq \Delta \quad (22)$$

where Δ is a positive constant.

To observe the state variables in (21), the third-order STSMO can be structured in the following form.

$$\begin{cases} \dot{\hat{x}}_1 = \hat{x}_2 + u - k_1 |e_1|^{2/3} sgn(e_1) \\ \dot{\hat{x}}_2 = \hat{\rho}_2(t) - k_2 |e_1|^{1/3} sgn(e_1) \\ \dot{\hat{\rho}}_2(t) = -k_3 sgn(e_1) \end{cases} \quad (23)$$

where the variables with the symbol "^" represent the corresponding estimations. The respective estimation error is defined as

$$\begin{cases} e_1 = \hat{x}_1 - x_1 \\ e_2 = \hat{x}_2 - x_2 \\ e_3 = \hat{\rho}_2(t) - \rho_2(t). \end{cases} \quad (24)$$

Then, subtracting (21) from (23), we can obtain the error equations as

$$\begin{cases} \dot{e}_1 = -k_1 |e_1|^{2/3} sgn(e_1) + e_2 \\ \dot{e}_2 = -k_2 |e_1|^{1/3} sgn(e_1) + e_3 \\ \dot{e}_3 = -k_3 sgn(e_1) - \dot{\rho}_2(t). \end{cases} \quad (25)$$

If $\rho_2(t)$ has a derivative with Lipschitz's constant $|\dot{\rho}_2(t)| \leq \Delta_1$, according to the conclusion in [35], the structured third-order STSMO is stable in finite time. In other words, e_1, e_2 and e_3 will quickly converge to zero in finite time if choosing some appropriate positive k_1, k_2 and k_3.

B. CURRENT AND DISTURBANCE ESTIMATION IN CURRENT LOOP

In (14), besides the current command coming from the output of the velocity controller, we also need to achieve the estimations of $I(k+1)$ and $D(k+1)$. In d-q axis rotating frame, based on the vector control of $i_d^* = 0$, i_q is proportional to the thrust force. So we take the q-axis current i_q and disturbance ζ_q as the example, and discuss their estimation method. According to (1), since the derivative of parameter disturbance is bounded, the state equations are expressed as

$$\begin{cases} \dot{i}_q = -\dfrac{R_o}{L_{qo}} i_q + \dfrac{v_q}{L_{qo}} - \dfrac{\pi v}{\tau L_{qo}} (L_{do} i_d + \lambda_{fo}) - \dfrac{\zeta_q}{L_{qo}} \\ \dot{\zeta}_q = \rho_3(t) \quad |\rho_3(t)| \leq \Delta \end{cases} \quad (26)$$

where $\rho_3(t)$ denotes the derivative of ζ_q.

Imitating the third-order STSMO in (23), when defining $x_1 = i_q$, $x_2 = -\zeta_q/L_{qo}$, and $x_3 = -\rho_3(t)/L_{qo}$, the equations to observe i_q and ζ_q are given as

$$\begin{cases} \dot{\hat{i}}_q = -\dfrac{R_o}{L_{qo}} i_q + \dfrac{v_q}{L_{qo}} - \dfrac{\pi v}{\tau L_{qo}} (L_{do} i_d + \lambda_{fo}) \\ \qquad - \dfrac{\hat{\zeta}_q}{L_{qo}} - k_1 |e_1|^{2/3} sgn(e_1) \\ \dot{\hat{\zeta}}_q = \hat{\rho}_3(t) + L_{qo} k_2 |e_1|^{1/3} sgn(e_1) \\ \dot{\hat{\rho}}_3(t) = L_{qo} k_3 sgn(e_1) \end{cases} \quad (27)$$

Make a subtraction between (27) and (26), the same error equations as (25) are obtained, which means the designed current and disturbance observer preserves the stability.

To utilize the third-order STSMO in PCC, by using the first-order Taylor series expansion method, the discrete-time equation of (27) is deduced as

$$\begin{cases} \hat{i}_q(k+1) = T_s \left[-\dfrac{R_o}{L_{qo}} i_q(k) + \dfrac{v_q(k)}{L_{qo}} \right. \\ \qquad \left. - \dfrac{\pi v(k)}{\tau L_{qo}} (L_{do} i_d(k) + \lambda_{fo}) \right] - \dfrac{T_s \hat{\zeta}_q(k)}{L_{qo}} \\ \qquad - T_s k_1 |e_1(k)|^{2/3} sgn(e_1(k)) + \hat{i}_q(k) \\ \hat{\zeta}_q(k+1) = T_s \hat{\rho}_3(k) + T_s L_{qo} k_2 |e_1(k)|^{1/3} sgn(e_1(k)) \\ \qquad + \hat{\zeta}_q(k) \\ \hat{\rho}_3(k+1) = T_s L_{qo} k_3 sgn(e_1(k)) + \hat{\rho}_3(k) \end{cases} \quad (28)$$

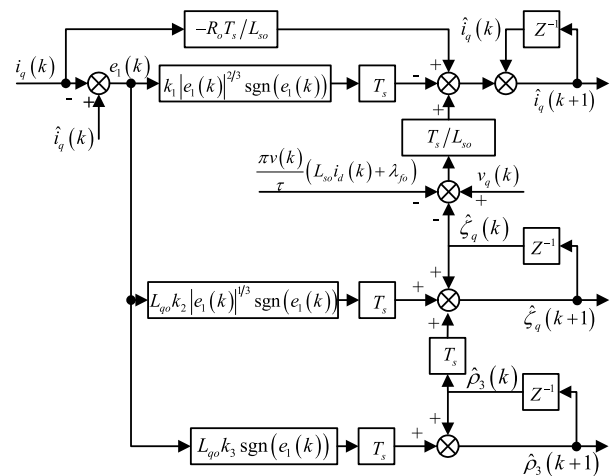To fully understand the third-order STSMO for i_q and ζ_q, its block diagram is depicted in Fig. 3.

FIGURE 3. Block diagram of the third-order STSMO for i_q and ζ_q.

C. DISTURBANCE ESTIMATION IN VELOCITY LOOP

For the output of the velocity controller, the force disturbance F_d has to be estimated. Since the parameter disturbance is naturally continuous, the derivative of disturbance is bounded. Based on (8), the state equations relating to v and F_d are

written as

$$\begin{cases} \dot{v} = \dfrac{k_f}{m}i_q + \dfrac{1}{m}F_d \\ \dot{F}_d = \rho_4(t) \quad |\rho_4(t)| \le \Delta \end{cases} \tag{29}$$

where $\rho_4(t)$ is the derivative of F_d.

Define $x_1 = v$, $x_2 = F_d/m$, and $x_3 = \rho_4(t)/m$, the third-order STSMO for F_d is designed as

$$\begin{cases} \dot{\hat{v}} = \dfrac{k_f}{m}i_q + \dfrac{1}{m}\hat{F}_d - k_1 |e_1|^{2/3} sgn(e_1) \\ \dot{\hat{F}}_d = \hat{\rho}_4(t) - mk_2 |e_1|^{1/3} sgn(e_1) \\ \dot{\hat{\rho}}_4(t) = -mk_3 sgn(e_1). \end{cases} \tag{30}$$

To realize the designed third-order STSMO for F_d in the digital system, it is necessary to discretize the observation equations.

$$\begin{cases} \hat{v}(k+1) = \dfrac{k_f T_s}{m}i_q(k) + \dfrac{T_s}{m}\hat{F}_d(k) \\ \qquad - T_s k_1 |e_1(k)|^{2/3} sgn(e_1(k)) + \hat{v}(k) \\ \hat{F}_d(k+1) = T_s \hat{\rho}_4(k) - T_s mk_2 |e_1(k)|^{1/3} sgn(e_1(k)) \\ \qquad + \hat{F}_d(k) \\ \hat{\rho}_4(k+1) = -T_s mk_3 sgn(e_1(k)) + \hat{\rho}_4(k). \end{cases} \tag{31}$$

To fully understand the third-order STSMO for F_d, its block diagram is depicted in Fig. 4.
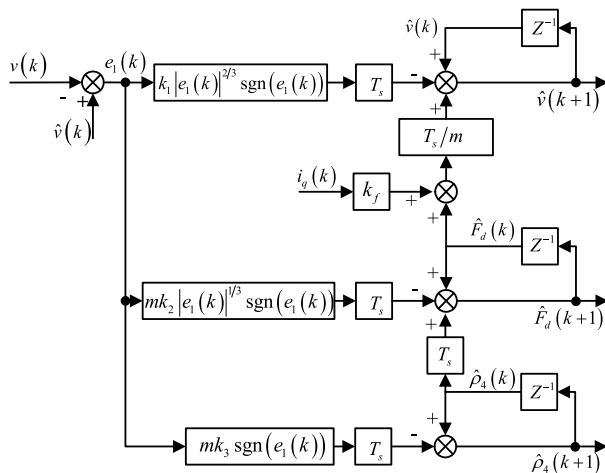

FIGURE 4. Block diagram of the third-order STSMO for F_d.

V. EXPERIMENTAL RESULTS

The overall experimental system shown in Fig. 5 consists of three parts, which are the iron core PMLSM, the inverter, and the upper computer. The PMLSM is supported by the aerostatic guide, therefore, the friction force can be ignored. The VSI with three sets of IGBTs is utilized to drive the PMLSM, and the control scheme is implemented by a Texas Instruments TMS320F28335 DSP, which is a 32-bit floating-point processor. The upper computer is used to collect and display the experimental data. Since the data in regard to the current

FIGURE 5. PMLSM drive platform.

loop are high dynamic, the data in current loop are displayed on the oscilloscope by a 12-bit DA converter. In addition, to accurately show the velocity tracking performance, the data with respect to the velocity loop are displayed on the upper computer. The switching and sampling frequency is set to 5 kHz, and the main motor parameters are given in Table 1.

TABLE 1. Main parameters of PMLSM.

Symbol	Values	Unit
τ	12	mm
R	6.5	Ω
L_s	35	mH
λ_f	0.24	Wb
m	45	kg
k_f	94.2	N/A

A. EXPERIMENTAL RESULTS IN CURRENT LOOP

For the control strategy in current loop, firstly, we give the ideal current tracking performance of the PCC under the parameter match condition. In this situation, the parameters set in the controller match the actual ones. Secondly, the current tracking results of the PCC without STSMO are shown when the parameters (resistance, inductance, and flux linkage) change with the motor running state, and the related adverse effects are discussed. By contrast, lastly, the results of the PCC with STSMO are given to verify the parameter robustness of the proposed scheme.
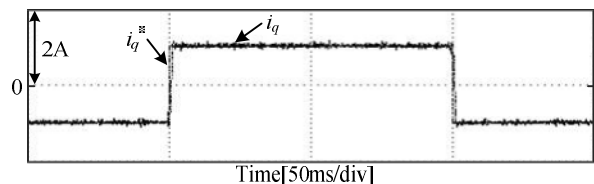

FIGURE 6. Ideal current tracking performance of the PCC.

When the parameters between the controller and the motor are equal, the current tracking performance of the PCC is perfect, as shown in Fig. 6. There is no steady-state error between the actual current and the command, and PCC has

a high static performance. In the meantime, the overshoot is close to zero, and the adjusting time is approximately equal to the response time. Therefore, the current controller based the PCC also has a high dynamic tracking performance.

In the working process, the motor parameters maybe changes with some conditions. For example, the resistance value increases as the temperature rises, and the flux linkage is not constant with the armature current change. Therefore, the tracking performance of the PCC will be degraded under the parameter variations. With the resistance variation $(R_o = 2R)$, it can be observed that there is a steady state error after the q-axis current stabilizes, as shown in Fig. 7(a). This error is proportional to the variation. With the inductance variation $(L_{so} = 2L_s)$, it is obvious that the dynamic performance is affected, as shown in Fig. 7(b), and the tracking current appears the oscillation, which must be eliminated in the actual system. In addition, with the fluxlinkage variation $(\lambda_{fo} = 2\lambda_f)$, the tracking error of the q-axis current gradually rises in the acceleration and deceleration process, as shown in Fig. 7(c).
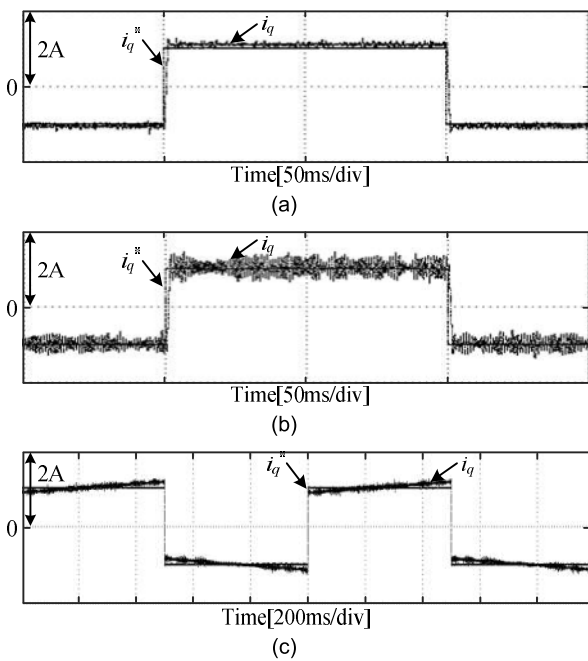

FIGURE 7. Current tracking performance of the PCC when the parameter variations. (a) $R_o = 2R$. (b) $L_{so} = 2L_s$. (c) $\lambda_{fo} = 2\lambda_f$.

According to the above results, the parameter disturbances really degrade the current control performance. To suppress these disturbances, Fig. 8 gives the compensation results under the parameter variations $(R_o = 2R, L_{so} = 2L_s, \lambda_{fo} = 2\lambda_f)$ with the proposed third-order STSMO. The observer coefficients are set as $k_1 = 40$, $k_2 = 14000$, and $k_3 = 50000$. It can be seen that the actual currents all can accurately track the command ones regardless of parameter variations. When $R_o = 2R$, there is no steady-state error as shown in Fig. 8(a), and the compensation voltage is about 6.5 [V]. When $L_{so} = 2L_s$, unlike the result in Fig. 7(b), the actual
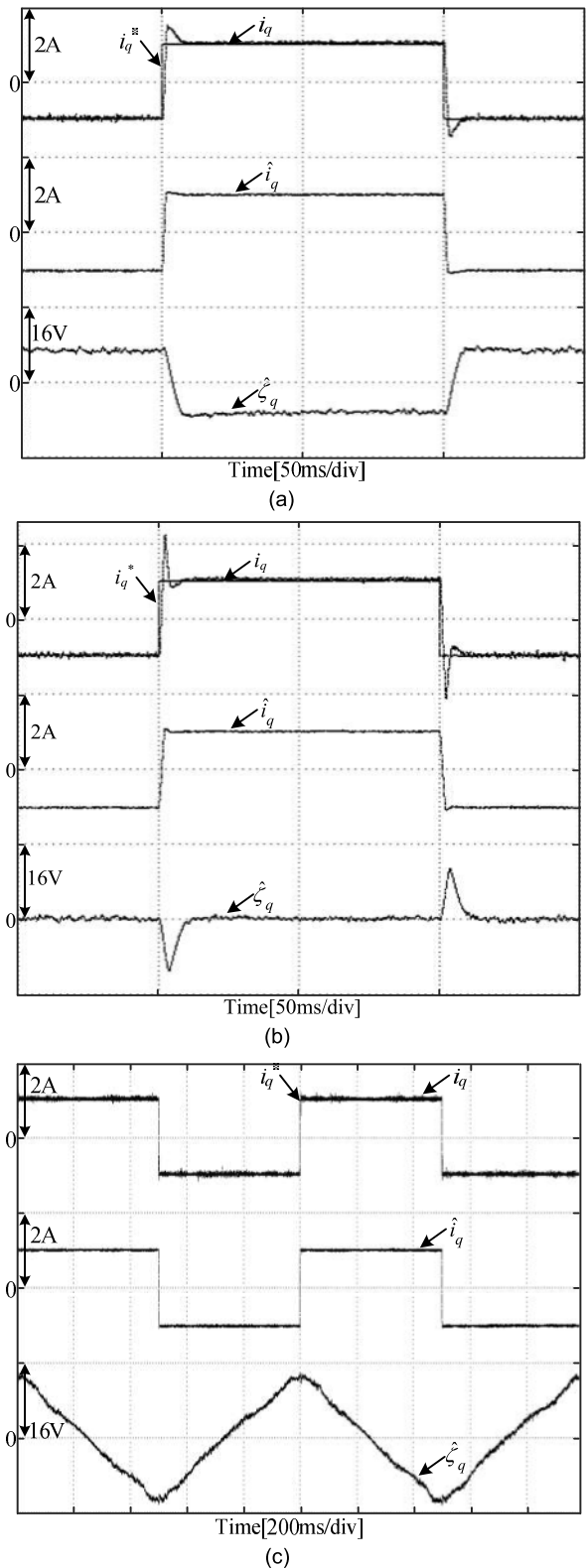

FIGURE 8. Current tracking performance of the PCC with the third-order STSMO when the parameter variations. (a) $R_o = 2R$. (b) $L_{so} = 2L_s$. (c) $\lambda_{fo} = 2\lambda_f$.

current in Fig. 8(b) will stabilize after a fast regulation, and there is no oscillation phenomenon. When $\lambda_{fo} = 2\lambda_f$, the actual current will not increase in the acceleration or

deceleration process, and the compensation voltage increases or decreases with the acceleration or deceleration. Therefore, the experimental results strongly verify the effectiveness of the proposed STSMO, and the parameter robustness of PCC is improved obviously.

B. EXPERIMENTAL RESULTS IN VELOCITY LOOP

For the control strategy in velocity loop, the comparison between the traditional PID and the proposed STSMC+STSMO is provided. The PID parameters according to the adjustment are tuned such as $k_p = 12$, $k_i = 0.01$, and $k_d = 8$. In the STSMC+STSMO, the control gains are set as $\alpha_1 = 1$, $\alpha_2 = 0.6$, and the observer parameters are given as $k_1 = 30$, $k_2 = 2000$, and $k_3 = 4000$.
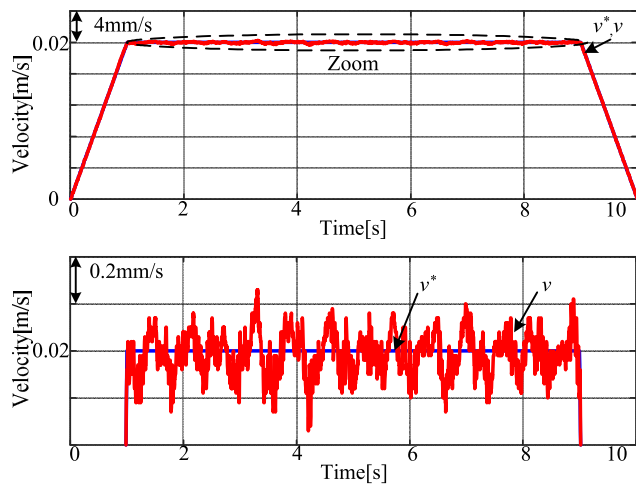

FIGURE 9. Velocity tracking performance of the PID control with the constant velocity of 0.02 m/s.

Fig. 9 shows the velocity tracking performance of the PID control. The velocity command is a trapezoidal trajectory, and the constant velocity is set as 0.02 m/s. By selecting the curve of the constant velocity to zoom in, it is clearly observed that there is a large tracking error, and the maximum of this error exceeds 0.2 mm/s. Compared with the PID control, the STSMC+STSMO has a good tracking performance and the tracking error is limited below 0.04 mm/s, as shown in Fig. 10(a). Fig. 10(b) illustrates the variation tendency of the estimated force disturbance. It is obvious that the disturbance has two components. One is the thrust ripple, which has the characteristic of the approximate periodicity. The thrust ripple is the main influence on the tracking precision, and its amplitude is about 7 N. Another one is the nonlinear cable force, which gradually changes with the mover motion. The error caused by the cable force can be effectively suppressed by the velocity closed-loop control. Therefore, through the control of the proposed STSMC+STSMO, the tracking precision is significantly improved.

To further justify the effectiveness of the proposed scheme, the tracking results with the different constant velocity are given as Fig. 11 and Fig. 12. It can be seen in Fig. 11 that the tracking error with the PID control is more than 0.4 mm/s
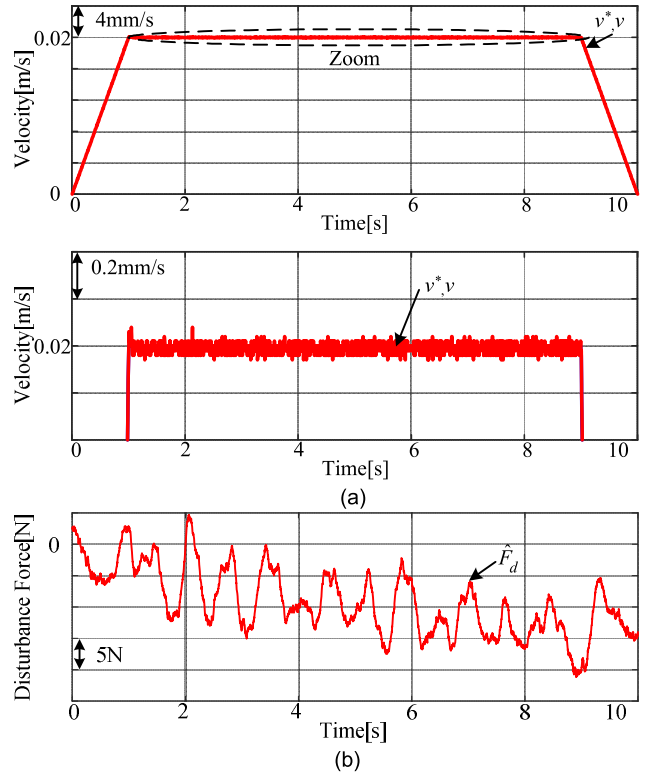

FIGURE 10. Velocity tracking performance of the proposed STSMC+STSMO with the constant velocity of 0.02 m/s. (a) Tracking curve. (2) Force disturbance estimation.
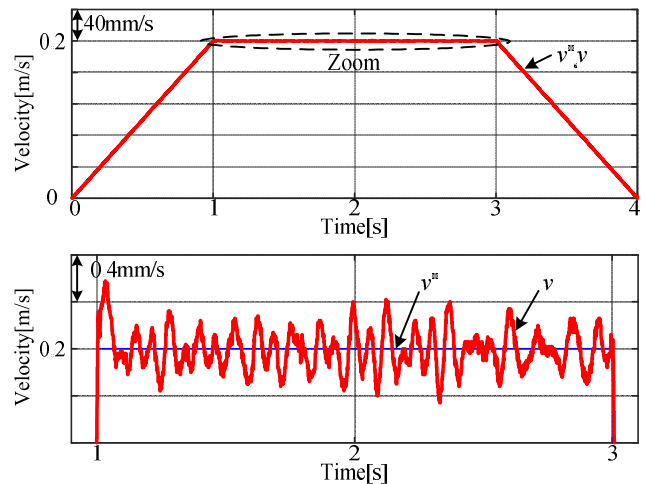

FIGURE 11. Velocity tracking performance of the PID control with the constant velocity of 0.2 m/s.

when the constant velocity is increased to 0.2 m/s. Similar to the result in Fig. 10, the tracking error is dramatically reduced by utilizing the proposed scheme, as shown in Fig. 12, and the tracking error is less than 0.1 mm/s during the constant velocity. The suppression effect of the force disturbance is limited by the convergence speed of the observer, so the tracking error is not absolutely eliminated, but the major portion of the force disturbance can be efficiently suppressed.
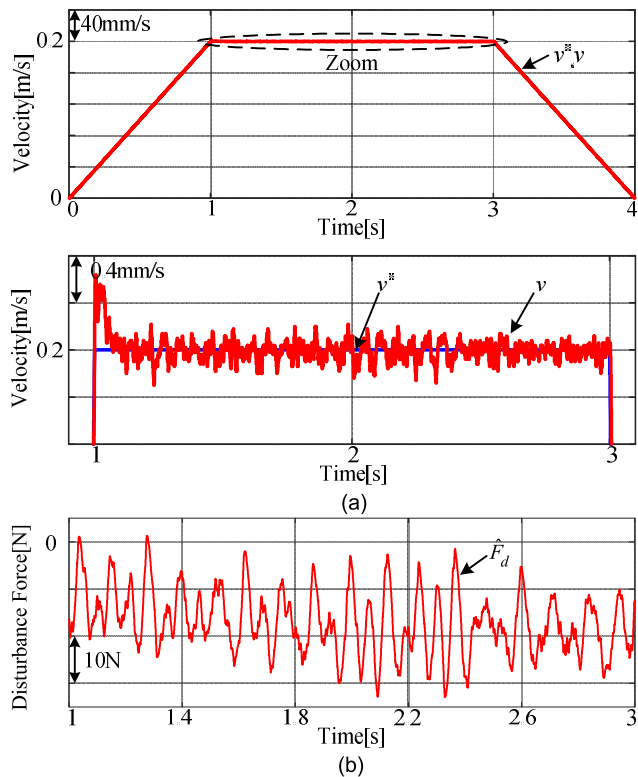
FIGURE 12. Velocity tracking performance of the proposed STSMC+STSMO with the constant velocity of 0.2 m/s. (a) Tracking curve. (2) Force disturbance estimation.

VI. CONCLUSION

This paper has proposed a double closed-loop control scheme with the strong robustness for PMLSM drives. The main contributions are summarized as follows: 1) to improve the dynamic and static performance, an improved PCC is presented; 2) a robust velocity loop control method based the super-twisting algorithm is adopted, and this method can avoid the chattering effect, which is different from the general SMC; 3) in order to overcome the parameter variation issue in current loop and suppress the force disturbance in velocity loop, the respective high-order STSMOs are structured. The experimental results justify that the proposed STSMC+PCC control scheme with STSMOs has higher tracking precision than the conventional PID control. However, the STSMO is limited by its convergence speed, and the force disturbance is difficult to be completely suppressed at a high velocity, which is considered to be the further research work.

REFERENCES

[1] C. Li, C. Li, Z. Chen, and B. Yao, "Advanced synchronization control of a dual-linear-motor-driven gantry with rotational dynamics," *IEEE Trans. Ind. Electron.*, vol. 65, no. 9, pp. 7526–7535, Sep. 2018.

[2] C. Hu, Z. Hu, Y. Zhu, and Z. Wang, "Advanced GTCF-LARC contouring motion controller design for an industrial X–Y linear motor stage with experimental investigation," *IEEE Trans. Ind. Electron.*, vol. 64, no. 4, pp. 3308–3318, Apr. 2017.

[3] H. Butler, "Magnetic disturbance compensation for a reticle stage in a lithographic tool," *Mechatronics*, vol. 23, no. 6, pp. 559–565, Sep. 2013.

[4] T. Mori, T. Hiramatsu, and E. Shamoto, "Simultaneous double-sided milling of flexible plates with high accuracy and high efficiency— Suppression of forced chatter vibration with synchronized single-tooth cutters," *Precis. Eng.*, vol. 35, no. 3, pp. 416–423, 2011.

[5] K. Sato, M. Katori, and A. Shimokohbe, "Ultrahigh-acceleration moving-permanent-magnet linear synchronous motor with a long working range," *IEEE/ASME Trans. Mechatronics*, vol. 18, no. 1, pp. 307–315, Feb. 2013.

[6] M. Wang, L. Li, and D. Pan, "Detent force compensation for PMLSM systems based on structural design and control method combination," *IEEE Trans. Ind. Electron.*, vol. 62, no. 11, pp. 6845–6854, Nov. 2015.

[7] F. Wu, F. Feng, L. Luo, J. Duan, and L. Sun, "Sampling period online adjusting-based hysteresis current control without band with constant switching frequency," *IEEE Trans. Ind. Electron.*, vol. 62, no. 1, pp. 270–277, Jan. 2015.

[8] M. P. Kazmierkowski and L. Malesani, "Current control techniques for three-phase voltage-source PWM converters: A survey," *IEEE Trans. Ind. Electron.*, vol. 45, no. 5, pp. 691–703, Oct. 1998.

[9] M. Wang, L. Li, D. Pan, Y. Tang, and Q. Guo, "High-bandwidth and strong robust current regulation for PMLSM drives considering thrust ripple," *IEEE Trans. Power Electron.*, vol. 31, no. 9, pp. 6646–6657, Sep. 2016.

[10] F. Morel *et al.*, "A comparative study of predictive current control schemes for a permanent-magnet synchronous machine drive," *IEEE Trans. Ind. Electron.*, vol. 56, no. 7, pp. 2715–2728, Jul. 2009.

[11] H.-T. Moon, H.-S. Kim, and M.-J. Youn, "A discrete-time predictive current control for PMSM," *IEEE Trans. Power Electron.*, vol. 18, no. 1, pp. 464–472, Jan. 2003.

[12] Y.-Y. Tzou and S.-Y. Lin, "Fuzzy-tuning current-vector control of a three-phase PWM inverter for high-performance AC drives," *IEEE Trans. Ind. Electron.*, vol. 45, no. 5, pp. 782–791, Oct. 1998.

[13] P. Wipasuramonton, Z. Q. Zhu, and D. Howe, "Predictive current control with current-error correction for PM brushless AC drives," *IEEE Trans. Ind. Appl.*, vol. 42, no. 4, pp. 1071–1079, Jul. 2006.

[14] A. Abbaszadeh, D. A. Khaburi, and J. Rodríguez, "Predictive control of permanent magnet synchronous motor with non-sinusoidal flux distribution for torque ripple minimisation using the recursive least square identification method," *IET Electr. Power Appl.*, vol. 11, no. 5, pp. 847–856, May 2017.

[15] K.-H. Kim, H.-S. Kim, and M.-J. Youn, "An improved stationary-frame-based current control scheme for a permanent-magnet synchronous motor," *IEEE Trans. Ind. Electron.*, vol. 50, no. 5, pp. 1065–1068, Oct. 2003.

[16] Y. A.-R. I. Mohamed and E. F. El-Saadany, "Robust high bandwidth discrete-time predictive current control with predictive internal model— A unified approach for voltage-source PWM converters," *IEEE Trans. Power Electron.*, vol. 23, no. 1, pp. 126–136, Jan. 2008.

[17] X. Zhang, B. Hou, and Y. Mei, "Deadbeat predictive current control of permanent-magnet synchronous motors with stator current and disturbance observer," *IEEE Trans. Power Electron.*, vol. 32, no. 5, pp. 3818–3834, May 2017.

[18] B. Wang, Y. Yu, G. Wang, and D. Xu, "Static-errorless deadbeat predictive current control using second-order sliding-mode disturbance observer for induction machine drives," *IEEE Trans. Power Electron.*, vol. 33, no. 3, pp. 2395–2403, Mar. 2018.

[19] D. Liang, J. Li, and R. Qu, "Sensorless control of permanent magnet synchronous machine based on second-order sliding-mode observer with online resistance estimation," *IEEE Trans. Ind. Appl.*, vol. 53, no. 4, pp. 3672–3682, Jul./Aug. 2017.

[20] Y. Jiang, W. Xu, C. Mu, and Y. Liu, "Improved deadbeat predictive current control combined sliding mode strategy for PMSM drive system," *IEEE Trans. Veh. Technol.*, vol. 67, no. 1, pp. 251–263, Jan. 2018.

[21] Y. S. Kung, C. C. Huang, and M. H. Tsai, "FPGA realization of an adaptive fuzzy controller for PMLSM drive," *IEEE Trans. Ind. Electron.*, vol. 56, no. 8, pp. 2923–2932, Aug. 2009.

[22] Z. Chen, B. Yao, and Q. Wang, "Adaptive robust precision motion control of linear motors with integrated compensation of nonlinearities and bearing flexible modes," *IEEE Trans. Ind. Informat.*, vol. 9, no. 2, pp. 965–973, May 2013.

[23] H. Ding and J. Wu, "Point-to-point motion control for a high-acceleration positioning table via cascaded learning schemes," *IEEE Trans. Ind. Electron.*, vol. 54, no. 5, pp. 2735–2744, Oct. 2007.

[24] F.-J. Lin, P.-K. Huang, and W.-D. Chou, "Recurrent-fuzzy-neural-network-controlled linear induction motor servo drive using genetic algorithms," *IEEE Trans. Ind. Electron.*, vol. 54, no. 3, pp. 1449–1461, Jun. 2007.

[25] F. J. Lin, P. H. Chou, C. S. Chen, and Y. S. Lin, "DSP-based cross-coupled synchronous control for dual linear motors via intelligent complementary sliding mode control," *IEEE Trans. Ind. Electron.*, vol. 59, no. 2, pp. 1061–1073, Feb. 2012.

[26] G. Sun and Z. Ma, "Practical tracking control of linear motor with adaptive fractional order terminal sliding mode control," *IEEE/ASME Trans. Mechatronics*, vol. 22, no. 6, pp. 2643–2653, Dec. 2017.

[27] Y. S. Huang and C. C. Sung, "Implementation of sliding mode controller for linear synchronous motors based on direct thrust control theory," *IET Control Theory Appl.*, vol. 4, no. 3, pp. 326–338, Mar. 2010.

[28] A. Levant, "Robust exact differentiation via sliding mode technique," *Automatica*, vol. 34, no. 3, pp. 379–384, Mar. 2010.

[29] A. Chalanga, S. Kamal, L. M. Fridman, B. Bandyopadhyay, and J. A. Moreno, "Implementation of super-twisting control: Super-twisting and higher order sliding-mode observer-based approaches," *IEEE Trans. Ind. Electron.*, vol. 63, no. 6, pp. 3677–3685, Jun. 2016.

[30] O. A. Morfin, C. E. Castañeda, A. Valderrabano-Gonzalez, M. Hernandez-Gonzalez, and F. A. Valenzuela, "A real-time SOSM super-twisting technique for a compound DC motor velocity controller," *Energies*, vol. 10, no. 9, pp. 1–18, Sep. 2017.

[31] S. Laghrouche, M. Harmouche, and Y. Chitour, "Higher order super-twisting for perturbed chains of integrators," *IEEE Trans. Autom. Control*, vol. 62, no. 7, pp. 3588–3593, Jul. 2017.

[32] M. Y. Wang, R. Yang, C. M. Zhang, J. W. Cao, and L. Y. Li, "Inner-loop design for PMLSM drives with thrust ripple compensation and high-performance current control," *IEEE Trans. Ind. Electron.*, vol. 65, no. 12, pp. 9905–9915, Mar. 2018.

[33] A. Levant, "Sliding order and sliding accuracy in sliding mode control," *Int. J. Control*, vol. 58, no. 6, pp. 1247–1263, Dec. 1993.

[34] J. A. Moreno and M. Osorio, "Strict Lyapunov functions for the super-twisting algorithm," *IEEE Trans. Autom. Control*, vol. 57, no. 4, pp. 1035–1040, Apr. 2012.

[35] J. A. Moreno, "A Lyapunov approach to second-order sliding mode controllers and observers," in *Proc. 47th IEEE Conf. Decis. Control*, Cancun, Mexico, Dec. 2008, pp. 2856–2861.

[36] F. A. Ortiz-Ricardez, T. Sánchez, and J. A. Moreno, "Smooth Lyapunov function and gain design for a second order differentiator," in *Proc. 54th IEEE Conf. Decis. Control*, Osaka, Japan, Dec. 2015, pp. 5402–5407.
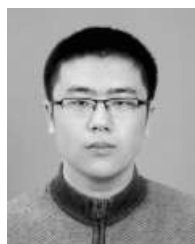
RUI YANG (S'16) was born in Hubei, China. He received the B.E. degree in electrical engineering from the Harbin Institute of Technology, Harbin, China, 2015, where he is currently pursuing the Ph.D. degree in electrical engineering.

His research interests include linear motor drive and control, predictive current control, adaptive control, and sliding mode control.

QIANG TAN received the B.E. and M.E. degrees in electrical engineering from the Nanjing University of Aeronautics and Astronautics, Nanjing, China, in 2014 and 2017, respectively. He is currently pursuing the Ph.D. degree with the Harbin Institute of Technology.

His current research interests include the design of linear permanent magnet synchronous motors.

JIA-LIN JIANG was born in Jiamusi, Heilongjiang, China. He received the B.E. degree in electrical engineering from the Harbin Institute of Technology, Harbin, China, in 2017, where he is currently pursuing the M.E. degree in electrical engineering.

His research interests include linear motor drive and control and sliding mode control.

MING-YI WANG was born in Jilin, China. He received the B.E., M.E., and Ph.D. degrees in electrical engineering from the Harbin Institute of Technology (HIT), Harbin, China, in 2009, 2011, and 2016, respectively.

He is currently with the Institute of Electromagnetic and Electronic Technology, HIT. His research interests include motor drive control, power electronic applications, and magnetic levitation.

LI-YI LI (M'09) received the B.E., M.E., and D.E. degrees from the Harbin Institute of Technology (HIT), Harbin, China, in 1991, 1995, and 2001, respectively. Since 2004, he has been a Professor with the School of Electrical Engineering and Automation, HIT.

In 2013, he became the Yangtze Fund Scholar Distinguished Professor and is currently supported by the National Science Fund for Distinguished Young Scholars. He has authored or co-authored over 110 technical papers and holds 50 patents. His research interests include the design, drive, and control of linear motors and the design and drive of high-speed/power density permanent magnet machines.

YU-JIE NIU was born in Changzhi, Shanxi, China. He received the B.E. degree in electrical engineering from the Harbin Institute of Technology, Harbin, China, in 2018, where he is currently pursuing the M.E. degree in electrical engineering.

His research interests include linear motor drive and control and sliding mode control.

• • •